



A novel framework for intelligent signal detection via artificial neural networks for cyclic voltammetry in pyroprocessing technology



Samaneh Rakhshan Pouri ^a, Milos Manic ^b, Supathorn Phongikaroon ^{a,*}

^a Department of Mechanical and Nuclear Engineering, Virginia Commonwealth University, Richmond, VA, USA

^b Department of Computer Science and Engineering, Virginia Commonwealth University, Richmond, VA, USA

ARTICLE INFO

Article history:

Received 1 June 2017

Received in revised form 25 August 2017

Accepted 1 September 2017

Keywords:

Simulation

ANN

Safeguards

Pyroprocessing

Cyclic voltammetry

Molten salt

ABSTRACT

Electrorefiner (ER) is the heart of pyroprocessing technology which contains different fission, rare-earth, and transuranic chloride compositions during the operation. This is still a developing technology that needs to be advanced for the commercial reprocessing design of used nuclear fuel (UNF) in terms of intelligent materials detection and accountability towards safeguards. A novel signal detection, artificial neural network (ANN), has been proposed in this study to apply on massive ER systemic parameters to simulate cyclic voltammetry (CV) graphs for the unseen situation. ANN could be trained to mimic the system by driving the data sets interrelation between variables to provide current and potential simulated data sets with a high accuracy of prediction. For this purpose, over 230,000 experimental data points reported in literature have been explored—0.5–5 wt% of zirconium chloride ($ZrCl_4$) in LiCl-KCl molten salt with different scan rates at 773 K. This study has illustrated a new framework of ANN implementation to eliminate trial and error approach by comparing the average error of one to three hidden layers with different number of neurons. In addition, this framework results in finding a preferable balance between underfitting and overfitting in deep learning. Furthermore, simulated CV graphs were compared with the experimental data and illustrated a reasonable prediction. The results reveal two structures with three hidden layers providing a good prediction with a low average error. The outcomes indicate that ANN has a strong potential in applying toward safeguards for pyroprocessing technology.

© 2017 Elsevier Ltd. All rights reserved.

1. Introduction

Pyroprocessing represents an alternative method for recycling Integral Fast Reactor fuel which separates the actinide elements from fission products (Laidler et al., 1997). This actinide recovery process of used nuclear fuel (UNF), which was initially developed at the Argonne National Laboratory (ANL), can be implemented via electrorefinery with dynamic compositions of molten salt during the process (Koch, 2008; Simpson and Law, 2010). For this purpose, the electrochemical behavior of actinide is necessary for a continuous monitoring routine. The composition analysis in ER can be measured by a common practice at the national laboratory level such as inductively coupled plasma mass spectrometry (ICP-MS). However, the extraction process, material transfer, and sample preparation may take up to several weeks due to radiation transferred process from the main operating facility to

radiochemistry laboratory and analytical preparation routines—these routines do not fulfill the near real time monitoring goal (Williams, 2016). Therefore, laser-induced breakdown spectroscopy (LIBS), Ultraviolet-visible spectroscopy (UV-Vis), and electrochemistry techniques (cyclic voltammetry (CV), chronopotentiometry, anodic stripping voltammetry, etc.) have been proposed as alternative techniques through the funding supports from the Department of Energy – Nuclear Energy University Program. These techniques can monitor the behavior of ER contains in the microsecond to 10 min; however, they still have some difficulties and are under developments.

One of the experimental electrochemical method which has been broadly utilized to measure thermodynamic behavior of uranium and zirconium within ER is CV (Evans et al., 1983; Kissinger and Heineman, 1983; Mabbott, 1983; Nicholson, 1965). This technique has been broadly proposed and utilized due to two main reasons: (1) its straightforwardness as a part of measuring apparent standard potentials, numbers of electrons transferred, and diffusion coefficients (Evans et al., 1983; Kissinger and Heineman, 1983; Mabbott, 1983) and (2) its simplicity in setup and fast

* Corresponding author.

E-mail addresses: rakhshapous@vcu.edu (S. Rakhshan Pouri), mmanic@vcu.edu (M. Manic), sphongikaroon@vcu.edu (S. Phongikaroon).

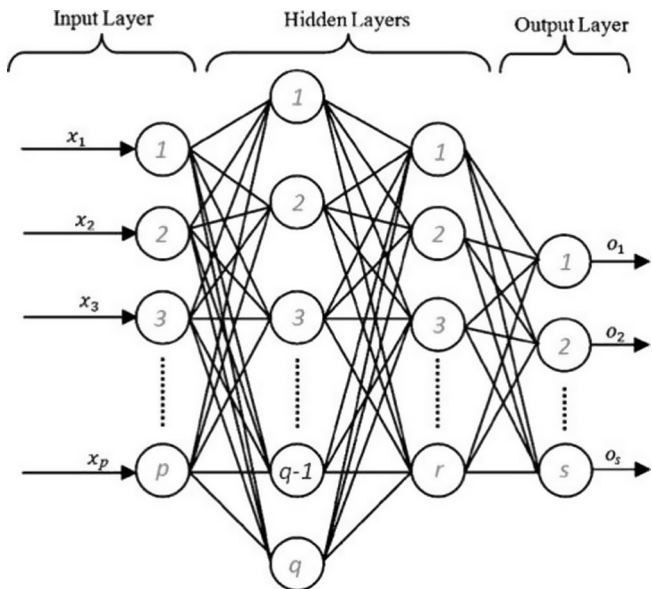


Fig. 1. Multi-layer perceptron schematic (Wijayasekara et al. (2011)).

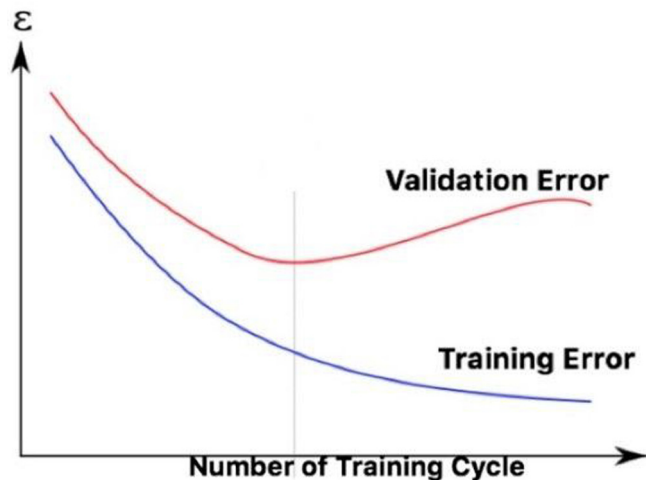


Fig. 2. Overfitting in learning (Burden and Winkler, 2009).

response time with functionality to directly evaluate reversibility and irreversibility for both the anodic and cathodic reactions of various species (Heinze, 1984; Nicholson, 1965; Oark et al., 2014).

Presently, there are several available commercial CV software packages providing the current versus potential diagram (for examples, Bio-logic EC-Lab, and Power CV). However, some of these packages cannot be used to trace different species without

experimental data sets in a relatively short time. Therefore, this issue has become a huge concern and a great need in improvement of nuclear material detection and accountancy (Hoover, 2014; Bio Logic Science Instrument, 2016). Although there are few (for example, BASiDigiSim Simulation) that have been developed to identify these species, analyses using them may require many hours to obtain the final outputs defeating the original purpose of a real time detection intention. Recently, two research teams have joined their effort to develop an analytical cyclic voltammetry study which uses a nonlinear least square procedure to fit a BET (multi-layer adsorption) model on the experimental data to trace the species. However, this study, which considered the adsorption effect of electrodes, is limited to a high standard reaction rate and similarity oxidant and reductant diffusivity. Also, the diffusion values calculated with the BET model were considerably larger than those with the Delahay equation (Samin et al., 2016, 2015).

The aforementioned issues provide a motivation to this study for developing an interactive modified diffusion method. To test its capability and methodology, zirconium (Zr), which was one of the major components in Experimental Breeder Reactor-II used metallic fuel was selected. In addition, due to the complexity in Zr cyclic voltammogram data sets, an artificial neural network (ANN) was proposed as another novel data analysis and simulation method that can be applied to electrochemical data sets and is inspired by brain neural neurons (Lahiri and Ghanta, 2010; Kriesel, 2007). Due to similarity between a computer machine and biological system, it has been discovered that the computer has its capability of learning by training samples (Kriesel, 2007). ANN can be implemented to learn massive training data set through iterations and interrelationships among system variables such as currents, potentials, concentrations, scan rates, processing times, and weight percent, without requiring the specific knowledge to predict the desire cyclic voltammetry (CV) graph which have not explicitly trained (Lahiri and Ghanta, 2010; Kriesel, 2007; Ridluan et al., 2009; Wijayasekara et al., 2011). One uniqueness of using ANN is its capability with non-linear, noisy, and uncertain data sets, which is invaluable for modeling, prediction, and optimization towards detection and material accountability in nuclear safeguards (Lahiri and Ghanta, 2010; Kriesel, 2007; Ridluan et al., 2009; Wijayasekara et al., 2011; Manic and Sabharwall, 2011).

Here, a huge experimental data set of 0.5–5 wt% of ZrCl₄ in LiCl-KCl eutectic molten salt at 773 K under different scan rates (over 231,000 data points) collected and reported by Hoover (2014) and Hoover et al. (2014) was being considered. ANN was implemented on the cyclic voltammetry (CV) to find a structure that provided a minimum error while predicting unseen data sets. All experimental runs that were conducted and reported by Hoover (2014) and Hoover et al. (2014) contained the following variables—potential, current, and time at specific concentration and scan rate. The overall goal was to determine the structures that

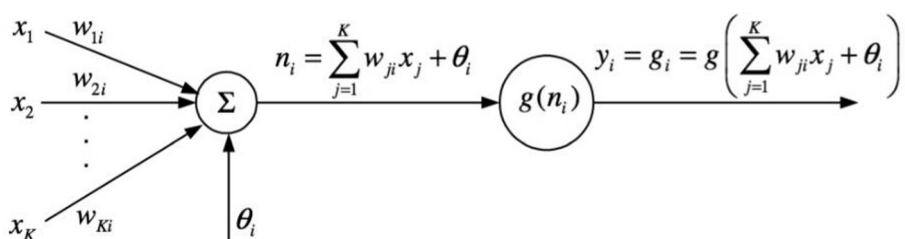


Fig. 3. A multilayer perceptron network with one hidden layer (Araromi and Afolabi, 2007).

ANN could be used to predict different systematic situations; the tasks were to determine (1) the minimum training data set requirement for achieving the lowest error, (2) the adequate numbers of hidden layers, (3) neurons at each layer, and (4) number of validation checks provides a minimum error. It was expected to apply this work to trace the operating current versus potential of a case with inadequate input information by interpolating between known information giving a low present error.

2. Methodology

The work was accomplished by implementing the ANN through the commercial software package, *Matlab*. One type of ANN that

has been used widely is called multi-layer perceptron (MLP). It is consisted of one input layer, various hidden layers and one output layer, which are interconnected by a number of nodes called neurons. Fig. 1 demonstrates the schematic of the MLP at ANN (Wijayasekara et al., 2011). Here, the experimental data sets (input data) were divided into three main parts: (1) training data set which was a partial of whole experimental data sets for adjusting the weights and bias; (2) validation data set which is an independent data set from training sample but can be regarded as a part of training data sets because it has been used in training phase to minimize the overtraining scheme; and (3) the leftover data sets were related to the test data sets to assess the system performance. Adding of additional hidden layer and increasing the number of

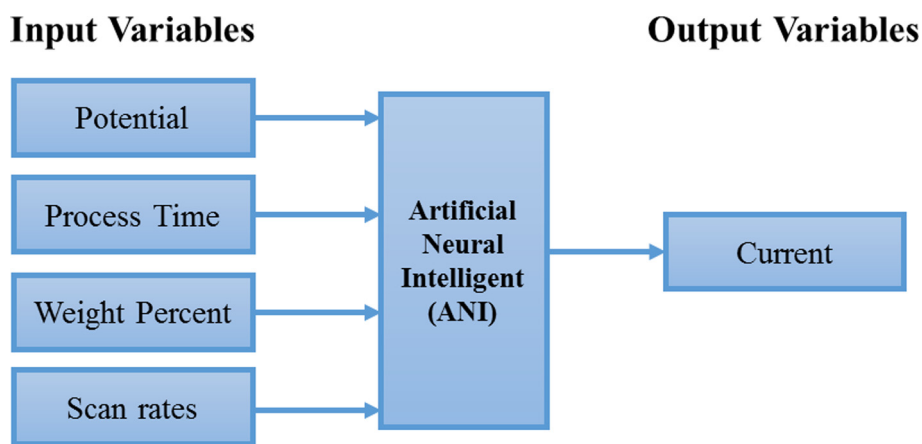


Fig. 4. Input and output variables of the ANN.

Table 1
Experimental data set for ZrCl₄ in LiCl-KCl at 773 K.

| Concentration (mol/cm ³) | Scan Rate (mV/s) Condition | | | | | | | | | | | | |
|---|-------------------------------|------|-------|------|-------|------|-------|-------|-------|-------|------|-------|--|
| | 200 | 250 | 300 | 350 | 400 | 450 | 500 | Train | Test | Train | Test | Train | |
| 0.5wt% | Train | Test | Train | Test | Train | Test | Train | | | | | | |
| | 150 | 150 | 200 | 200 | 250 | 250 | 300 | 300 | 350 | 350 | 350 | | |
| 1wt% | Train | Test | Train | Test | Train | Test | Train | Test | Train | Test | Test | | |
| | 100 | 100 | 150 | 200 | 250 | 300 | 300 | 400 | 500 | 500 | 500 | | |
| 2.5wt% | 50 | 50 | 100 | 100 | 150 | 150 | 200 | 200 | 200 | 250 | 250 | 300 | |
| | Train | Test | Train | Test | Train | Test | Train | Test | Train | Test | Test | Test | |
| 5wt% | 50 | 50 | 100 | 100 | 150 | 150 | 200 | 200 | 200 | 250 | 250 | 300 | |
| | Train | Test | Train | Test | Train | Test | Train | Test | Train | Test | Test | Test | |

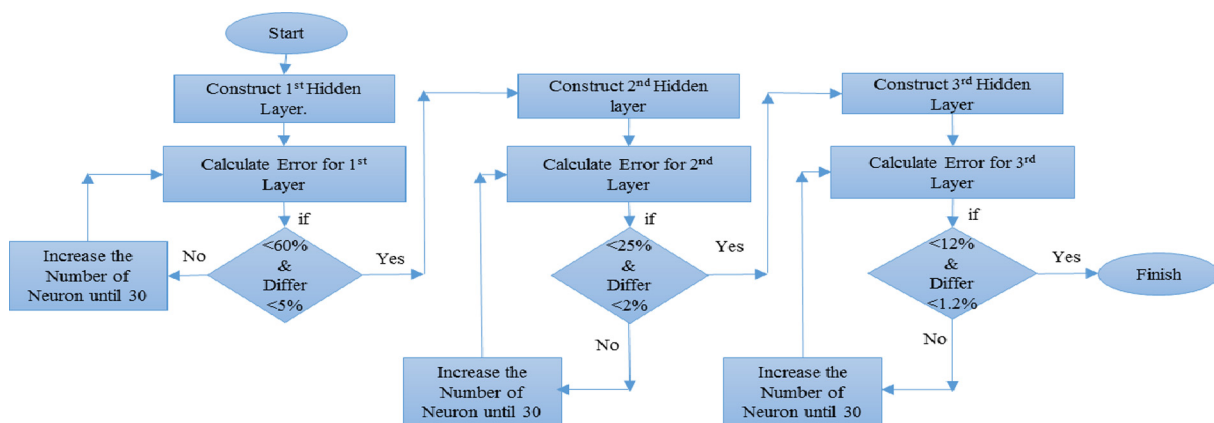


Fig. 5. Procedure flow chart showing ANN scheme finding hidden layers.

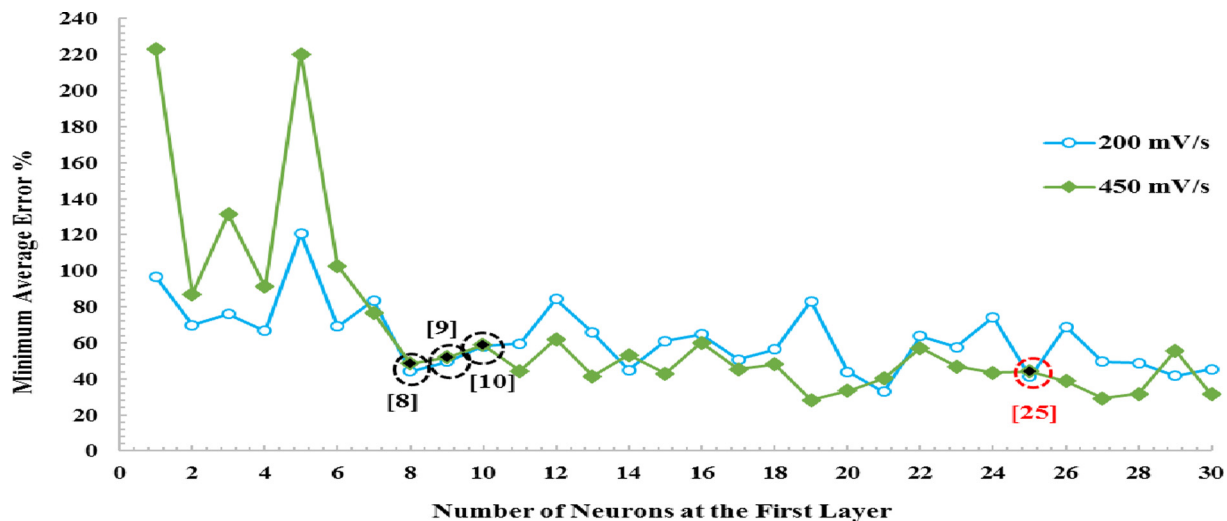


Fig. 6. One hidden layer with 1–30 neurons and 1–30 validation checks for 0.5 wt% at 200 mV/s and 450 mV/s (Black circle = short simulation time; Red circle = long simulation time). (For interpretation of the references to colour in this figure legend, the reader is referred to the web version of this article.)

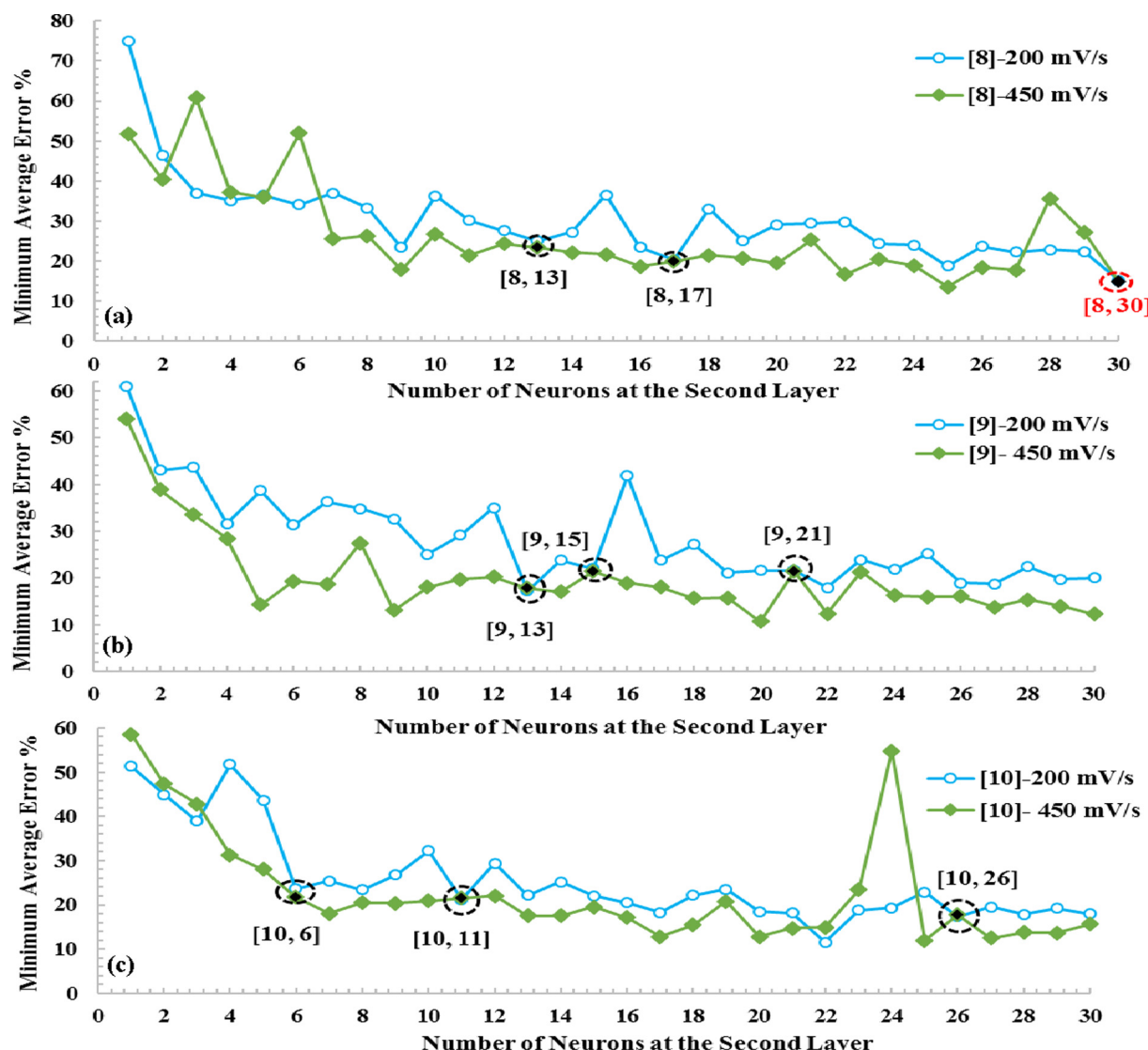


Fig. 7. Two hidden layers with 1–30 neurons and 1–30 validation checks for 0.5 wt% at 200 mV/s and 450 mV/s in three structures; (a) [8, 1–30], (b) [9, 1–30], and (c) [10, 1–30] (Black circle = short simulation time; Red circle = long simulation time). (For interpretation of the references to colour in this figure legend, the reader is referred to the web version of this article.)

neurons within each layer enhanced the neural network complexity is expected to improve prediction resulting in a lower error for a fixed training data set. It is important to consider that if the number of layers goes up to four layers in this study, the overfitting can occur and the run time increases significantly, therefore defeating the purpose of achieving a fast and robust detection method. For this reason, several validation checks have been considered representing the number of consecutive iterations that system performance fails to decrease and it is different from the total iterations of system training. The use of validation here was related to ANN assessment and should not be confused by verification and validation (V&V) (Taylor et al., 2003). In theory, overfitting happens when the system begins to memorize the training data set rather than learning (Siriphala, 2000); that is, the validation error starts to increase after an optimal situation (see Fig. 2) and the training error goes down gradually while the test error increases progressively (Lawrence et al., 1997; Baskin et al., 2006). Fig. 2 shows that the best predictive model is where the validation error (ε) reaches a global minimum (Burden and Winkler, 2009; Gardner and Dorling, 1998).

Here, inputs with the MLP network were weighted (w_{ji}) and summed up with the constant bias term (b_i), as shown in Fig. 3. This approach yielded the resulting data (n_i) input to the activation

function ($g(n_i)$), giving the outputs (y_i) (Araromi and Afolabi, 2007). It is important to mention that each experimental data set is consisted of the following variables—potential, process time, concentrations and scan rates as the input data and current as the output. The input and output variables are shown in Fig. 4. The hidden layer comprised of neurons arrays that received, transformed, and transferred the signal from the previous layer. The signals from the input and hidden layer to the output layer were modeled by an activation function which was generally linear, hyperbolic tangent, and sigmoid (Planche and Cordeiro, 2015). The ANN feature in the Matlab software was written based on the sigmoid function of these hidden layers.

Over the recent decades, various algorithms for determining the network parameters such as weight values have been developed. Based on the literature reported, the most well-known are back-propagation algorithm (BPA) and Levenberg-Marquardt algorithm (LMA). Here, LMA is more efficient due to its fast process time and can provide an adequate way for curve-fitting problems because of interpolating between two method of Gauss-Newton algorithm (GNA) and Gradient Descent (Araromi and Afolabi, 2007; Gavin, 2016). The gradient descent method can be used to find a local minimum of a function by reducing the sum of the squared errors with updating the parameters in the steepest-

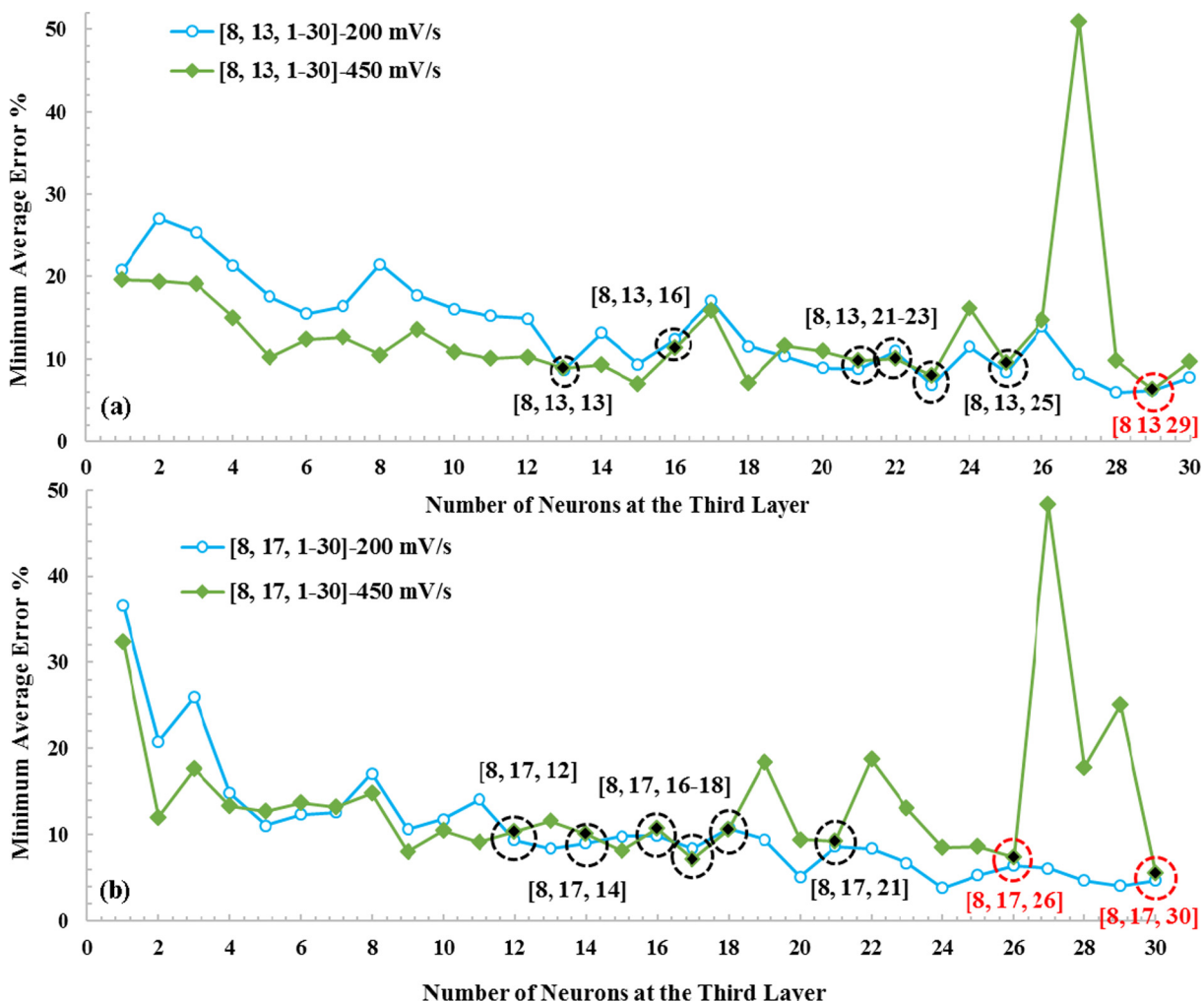


Fig. 8. Three hidden layers with 1–30 neurons and 1–30 validation checks for 0.5 wt% at 200 mV/s and 450 mV/s in three structures; (a) [8, 13, 1–30], and (b) [8, 17, 1–30] (Black circle = short simulation time; Red circle = long simulation time). (For interpretation of the references to colour in this figure legend, the reader is referred to the web version of this article.)

descent direction. However, the sum of the squared errors in the Gauss-Newton method is reduced by assuming that the least squares function is locally quadratic—finding the minimum of the quadratic (Araromi and Afolabi, 2007).

Because this work focused on the minimum number of training data that could provide a reasonable predicted error, different training combinations have been explored. It was found that this

work could be implemented with 43% of total experimental data set at a specific and fix combination. These results are listed in Table 1 keeping in mind that the total experimental data points are over 230,000 consisting of the potential, current, and process time for different Zr concentrations and scan rates. It should be noted that some conditions are being repeated two to three times (see Table 1). The training data sets are pointed in shade and the

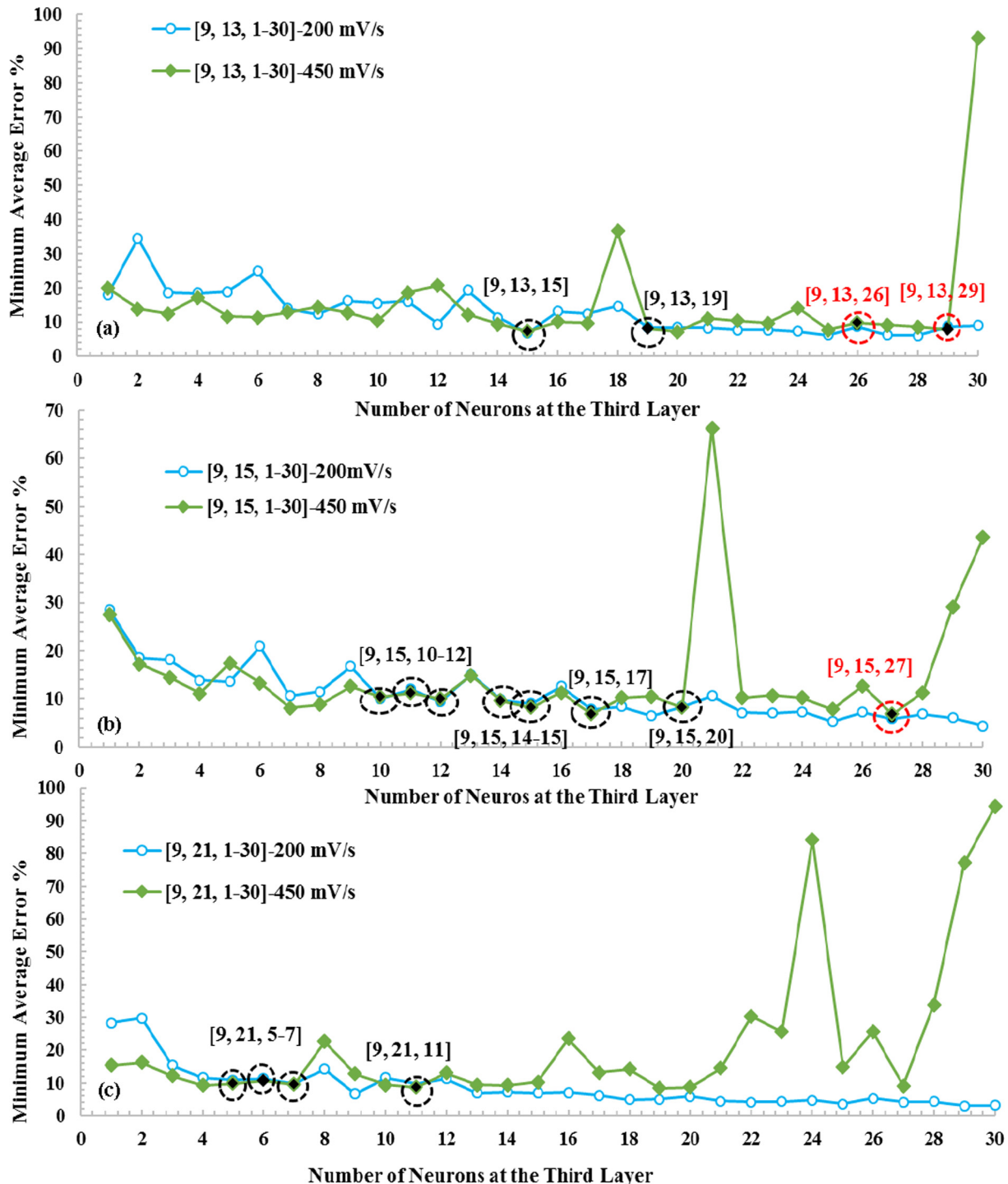


Fig. 9. Three hidden layers with 1–30 neurons and 1–30 validation checks for 0.5 wt% at 200 mV/s and 450 mV/s in three structures; (a) [9, 13, 1–30], (b) [9, 15, 1–30], (c) [9, 21, 1–30] (Black circle = short simulation time; Red circle = long simulation time). (For interpretation of the references to colour in this figure legend, the reader is referred to the web version of this article.)

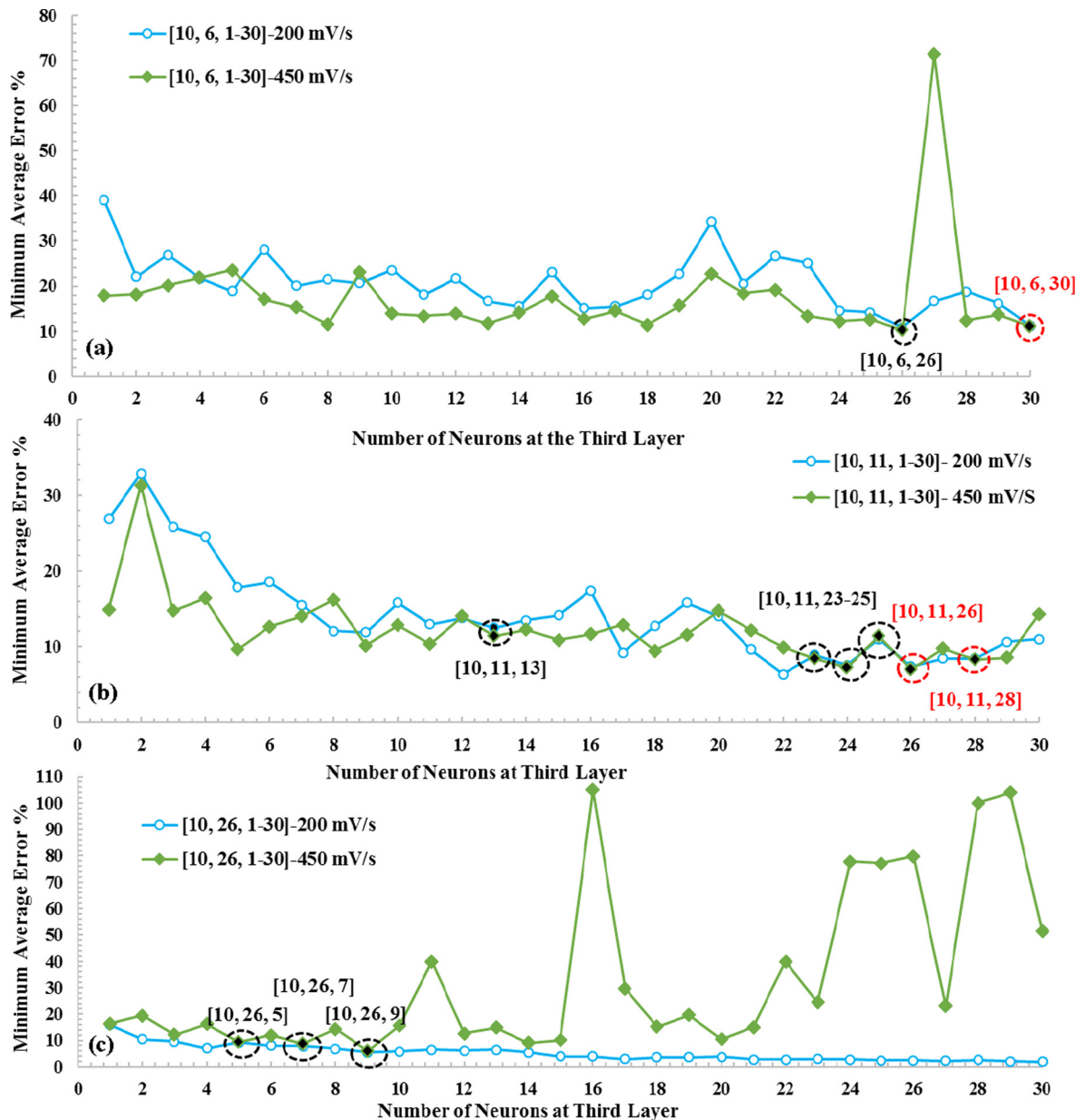


Fig. 10. Three hidden layers with 1–30 neurons and 1–30 validation checks for 0.5 wt% at 200 mV/s and 450 mV/s in three structures; (a) [10, 6, 1–30], (b) [10, 11, 1–30], and (c) [10, 26, 1–30] (Black circle = short simulation time; Red circle = long simulation time). (For interpretation of the references to colour in this figure legend, the reader is referred to the web version of this article.)

Table 2
Final results related to Figs. 8–10.

| | 200 mV/s Min Ave Error % | 450 mV/s Min Ave Error % | Validation Checks | 200 mV/s Min Ave Error % | 450 mV/s Min Ave Error % | Validation Checks |
|------------------|--------------------------|--------------------------|-------------------|--------------------------|--------------------------|-------------------|
| [8 13 13] | 12 | 8 | 16 | [9 15 11] | 12 | 15 |
| [8 13 16] | 12.29 | 20.58 | 11 | [9 15 14] | 9.8 | 49 |
| [8 13 21] | 16.44 | 9.82 | 27 | [9 15 15] | 15 | 8 |
| [8 13 22] | 12.86 | 10.05 | 5 | [9 15 17] | 7.80 | 16 |
| [8 13 25] | 16.16 | 9.52 | 9 | [9 15 20] | 8.76 | 12.22 |
| [8 17 7] | 12.50 | 14.74 | 16 | [9 21 5] | 10.85 | 44 |
| [8 17 12] | 9 | 14 | 28 | [9 21 6] | 28.86 | 10.74 |
| [8 17 14] | 22.43 | 10 | 21 | [9 21 7] | 9.72 | 9.32 |
| [8 17 16] | 13.76 | 10.69 | 23 | [9 21 11] | 12.97 | 8.58 |
| [8 17 17] | 8.35 | 12.22 | 15 | [10 11 13] | 12.43 | 12.7 |
| [8 17 18] | 10.74 | 21.15 | 15 | [10 11 23] | 9 | 16 |
| [8 17 21] | 41.52 | 9.21 | 17 | [10 11 25] | 11 | 11 |
| [9 13 15] | 6.70 | 12 | 19 | [10 26 5] | 18.16 | 9.24 |
| [9 13 19] | 8.45 | 11.90 | 30 | [10 26 7] | 7.84 | 8.81 |
| [9 15 10] | 9.94 | 10.30 | 18 | [10 26 9] | 26.69 | 6.04 |

test data sets are indicated in clear-white. Two conditions of 0.5 wt % at 200 and 450 mV/s are considered as train and test samples for further discussion.

The framework proposed in this paper entailed running ANN on different hidden layers (1–3) with various neurons (1–30) at several validation checks (1–30). The ANN routine was applied on one hidden layer with different neurons and each at different validation checks. The general schematic flow diagram of the compu-

tational procedures is shown in Fig. 5. The average percent error between experimental and predicted data sets for 0.5 wt% at 200 and 450 mV/s was calculated, as the train and the test samples, respectively. Then, the structure of both cases (200 and 450 mV/s) that provided a minimum average percent error was selected. The mean absolute percentage error (MAPE) between experimental and predicted data sets for 0.5 wt% at 200 and 450 mV/s was calculated using the following expression:

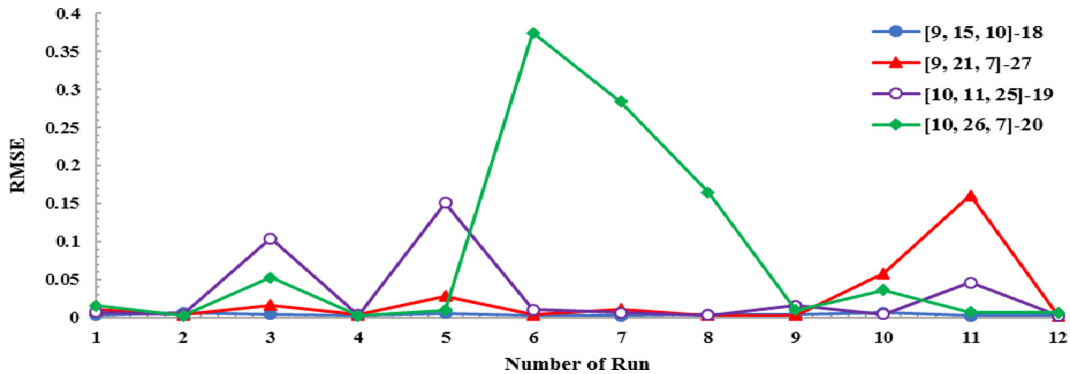


Fig. 11. RMSE of test sample for four final structures with 12 runs.

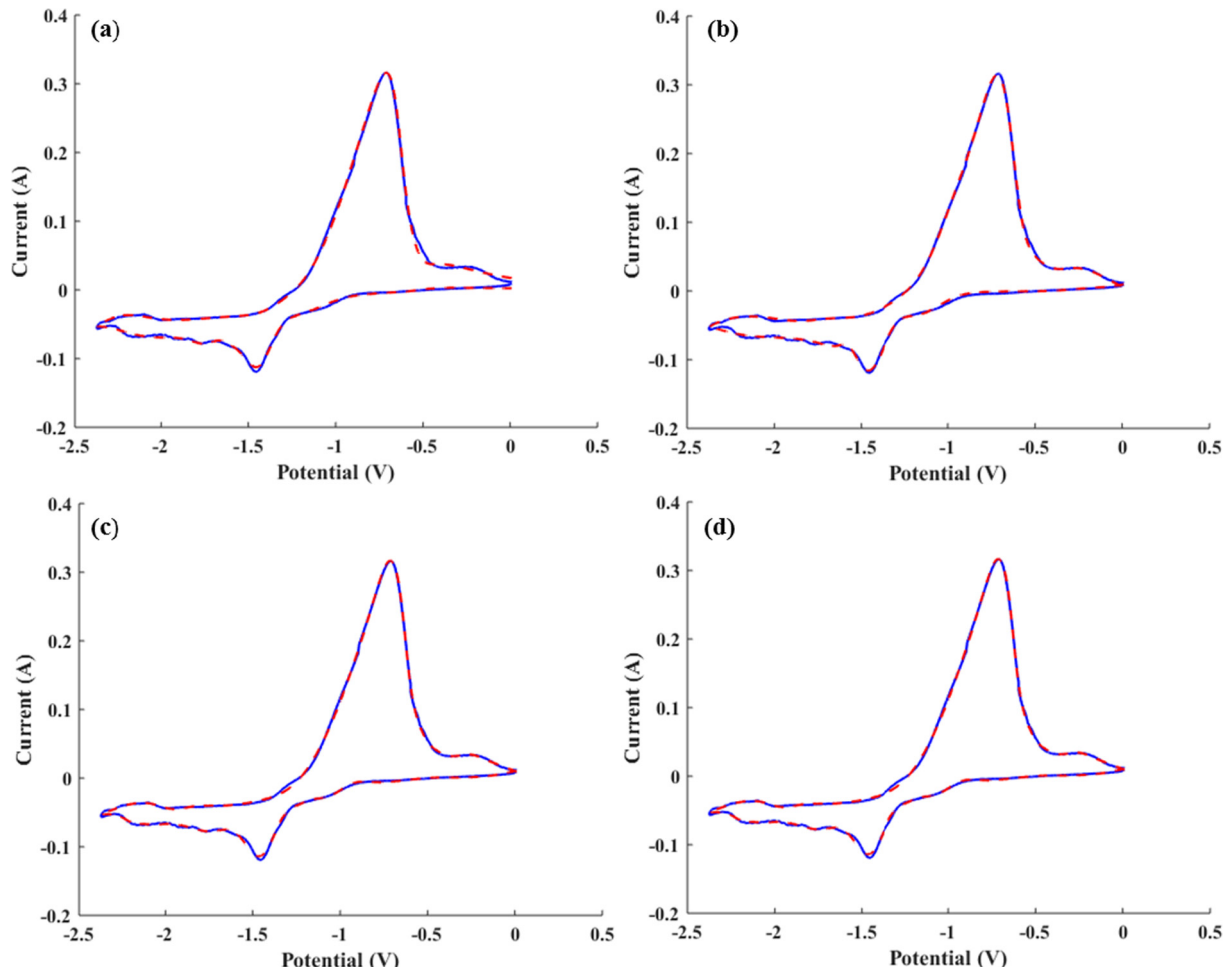


Fig. 12. Comparison of CV plot for 0.5 wt% ZrCl₄ at 200 mV/s, (a): [9, 15, 10]-18 (b): [9, 21, 7]-27, (c): [10, 11, 25]-19, (d): [10, 26, 7]-20 (Blue line = experimental data, Red dash line = ANN prediction). (For interpretation of the references to colour in this figure legend, the reader is referred to the web version of this article.)

$$MAPE = \frac{100}{n} \sum_{t=1}^n \left| \frac{ActualValue_t - ForecastValue_t}{ActualValue_t} \right| \quad (1)$$

Next, the number of hidden layer was increased to two and three layers following the same procedure. Thus, the situation that gave almost the same minimum average percent errors for both 200 and 450 mV/s would be used to generate the predicted CV plots for comparison and reliability with the existing experimental data sets.

3. Results and discussion

3.1. Determination of the first, second and third hidden layers

Fig. 6 shows the comparisons between minimum average percent errors of one hidden layer with various number of neurons and validation checks for 200 and 450 mV/s. Here, the minimum average error for one neuron at the first hidden layer with 1–30 validation checks for 200 and 450 mV/s are 96%, and 222%, respectively. The errors decrease to 45%, and 31% for 30 neurons at 200 mV/s and 450 mV/s, respectively. The points that both considered train and test samples provide the average error less than 60% while the deviations are less than 5% have been marked by the dashed circles. It can be seen that 8, 9, 10, and 25 neurons at the first layer (indicated by [8], [9], [10], and [25]) meet the mentioned

criteria. It is important to mention that enhancing the number of neurons will increase the processing time. For example, processing time of the first layer with 30 validation checks for 1 and 30 neurons are about 18 s and 8 min, respectively. The long processing time is the reason why the 25 neurons (see the red-dashed circle in **Fig. 6**), is not being considered for the second layer study.

To investigate the second hidden layer, the results from first hidden layer were selected as the starting point. First, we considered the case of having 8 neurons at the first hidden layer and 1–30 neurons at the second layer, denoted by [8, 1–30], with 1–30 validation checks. The points that provide average percent errors less than 25% for both 200 and 450 mV/s while having the difference around 2% are marked in **Fig. 7**. The results indicate that [8, 13], [8, 17], and [8, 30] fall within the criteria. Here, the processing time for [8, 1] at 30 validation checks is approximately 9 min and increases up to ~31 min for the [8, 30]. Therefore, the [8, 30] case was not selected for the third hidden layer study. As indicated in **Fig. 7(b)–(c)**, [9, 13], [9, 15], [9, 21], [10, 6], [10, 11], and [10, 26] meet the mentioned criteria and can be considered for the next hidden layer.

All the selected results from the two layers were further studied for the third hidden layer. Criteria in this part were to select the points that both train and test samples would yield an average error below 12% with a difference of 1.2%; **Fig. 8** displays the errors for [8, 13] and [8, 17], respectively. In addition, the [9, 13], [9, 15], [9, 21], [10, 6], [10, 11], and [10, 26] are shown in **Figs. 9 and 10**.

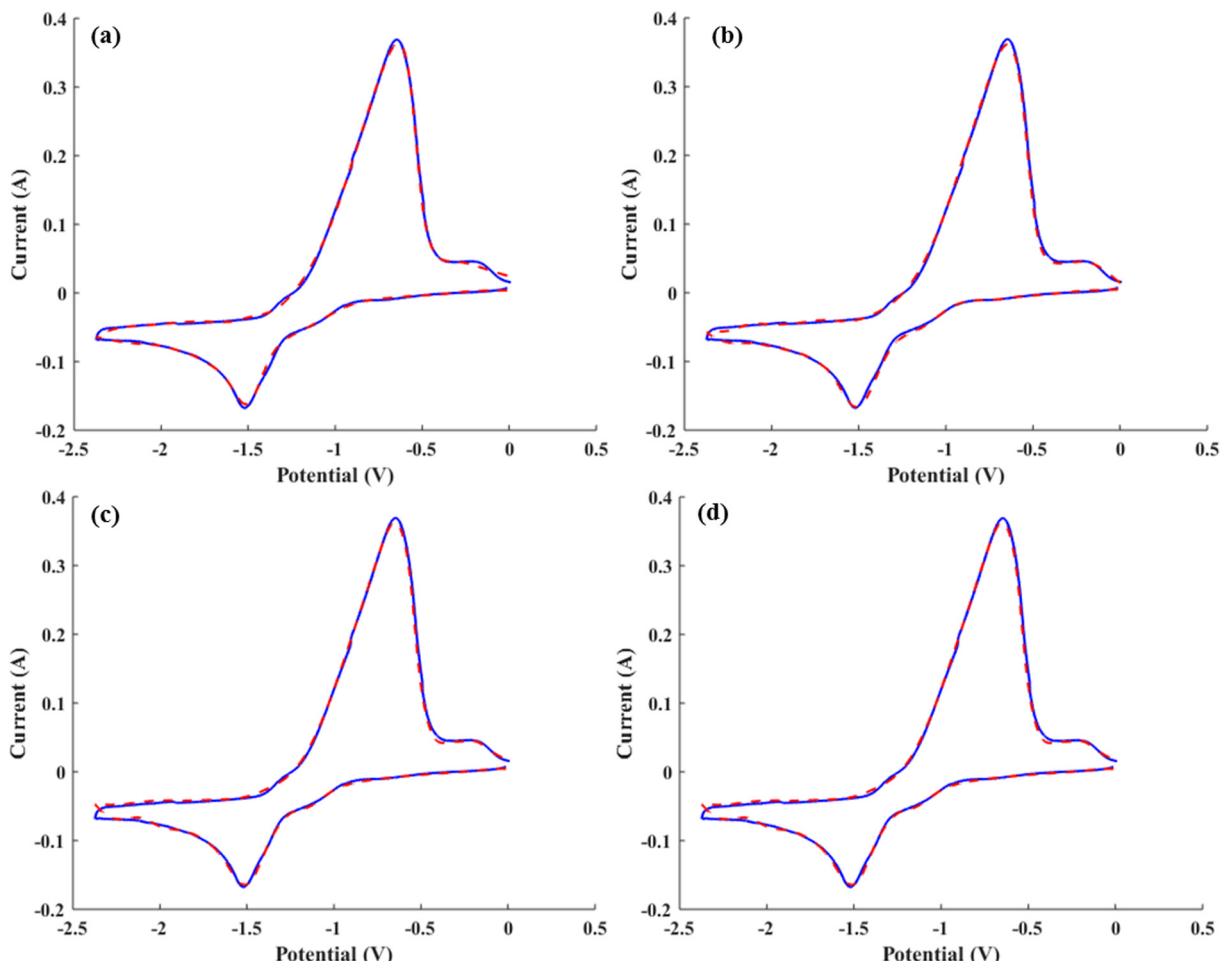


Fig. 13. Comparison of CV plot for 0.5 wt% ZrCl₄ at 450 mV/s, (a): [9, 15, 10]-18 (b): [9, 21, 7]-27, (c): [10, 11, 25]-19, (d): [10, 26, 7]-20 (Blue line = experimental data, Red dash line = ANN prediction). (For interpretation of the references to colour in this figure legend, the reader is referred to the web version of this article.)

The red circles indicate that these structures have not been considered as the final results due to their long processing times.

Each point mentioned in Figs. 8–10 are related to a specific validation check. For example, the train and test sample points for [10, 26, 5] structure in Fig. 10 are occurred at 21 and 17 validation checks, respectively; this give the minimum average error of ~9%. Therefore, to select the proper validation check for [10, 26, 5] structure, we would routinely swab the validation checks to assure the average minimum error. That is, the train sample points for [10, 26, 5] structure would be verified by 17 validation checks and vice versa. The results of this reversal technique show the average error percent for train (using 17 validation checks) and test samples (using 21 validation checks) are 18% and 31%, respectively. Thus, by selecting the [10, 26, 5] with 17 validation checks, the average error for train and test samples are, 18% and 9%, respectively. These results yield a lower error in comparison to 21 validation checks. This approach was applied for all final results (black circles) in Figs. 8–10 (all values are listed in Table 2). The structures that provide at most 11% error for both 200 and 450 mV/s cases with a difference about 1% are underlined and bolded in Table 2. The final results satisfying the mentioned criteria are as follows: [9, 15, 10]-18, [9, 21, 7]-27, [10, 11, 25]-19, and [10, 26, 7]-20. We will refer to these results as the 'final structure [a, b, c]-d' where a, b, and c are the number of neurons in each layer, and d is the number of validation checks.

It should be noted that the predicted results are not the same by repeating one structure because of randomly selected weights and biases by the computer. Therefore, each four final structures were repeated 12 times to compare the predicted values errors for the test sample (0.5 wt%, 450 mV/s). Fig. 11 shows that the root mean square error (RMSE) values for predicted out comes with structure [9, 15, 10]-18 are consistently maintaining at the same range in comparison to other structures. The average RMSE values of 12 runs for the test sample illustrated in Fig. 11 with four mentioned structures are within 0.004 and 0.081 while those for train samples (0.5 wt% at 200 mV/s) are ranging from 0.002 to 0.0032. To further prove this novel scheme, the final results were used to generate the CV plots for comparison to actual experimental data sets.

3.2. CV comparison

The CV plots of the four final structures with three hidden layers are being compared with experimental data sets (Figs. 12–16) based on the discussion in the previous section. Two distinctive colors are used to distinguish the experimental data collected by Hoover (2014) and Hoover et al. (2014) (blue line) and the ANN prediction (red dash line). Figs. 12 and 13 illustrate the comparison of four cases for train and test samples. Here, it can be seen that simulated CV curves based from all final four structures capture unique feature of both train and test conditions well. In addition,

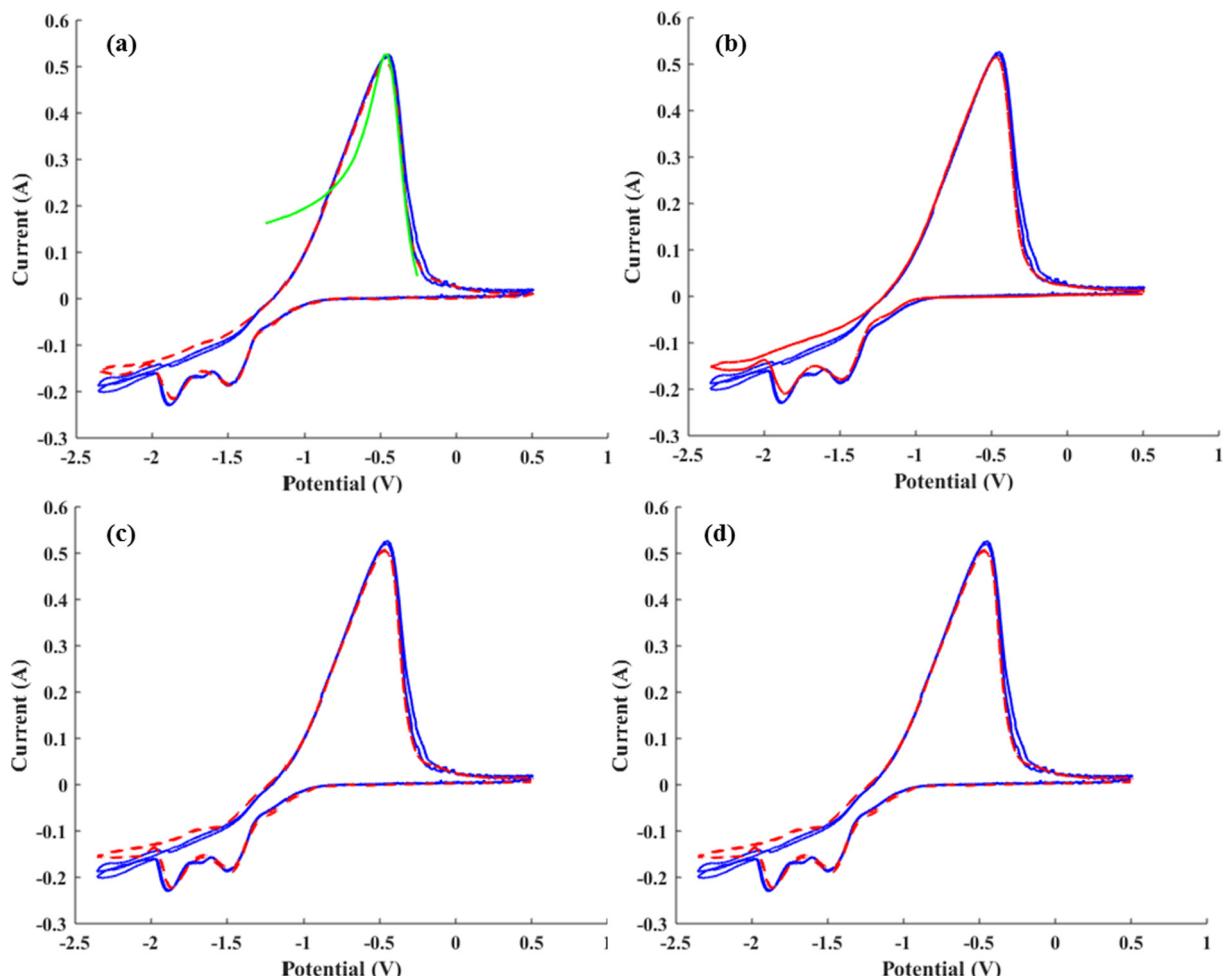


Fig. 14. Comparison of CV plot for 1 wt% ZrCl₄ at 300 mV/s. (a): [9, 15, 10]-18 (b): [9, 21, 7]-27, (c): [10, 11, 25]-19, (d): [10, 26, 7]-20 (Blue line = experimental data, Red dash line = ANN prediction, Green line = Diffusion model). (For interpretation of the references to colour in this figure legend, the reader is referred to the web version of this article.)

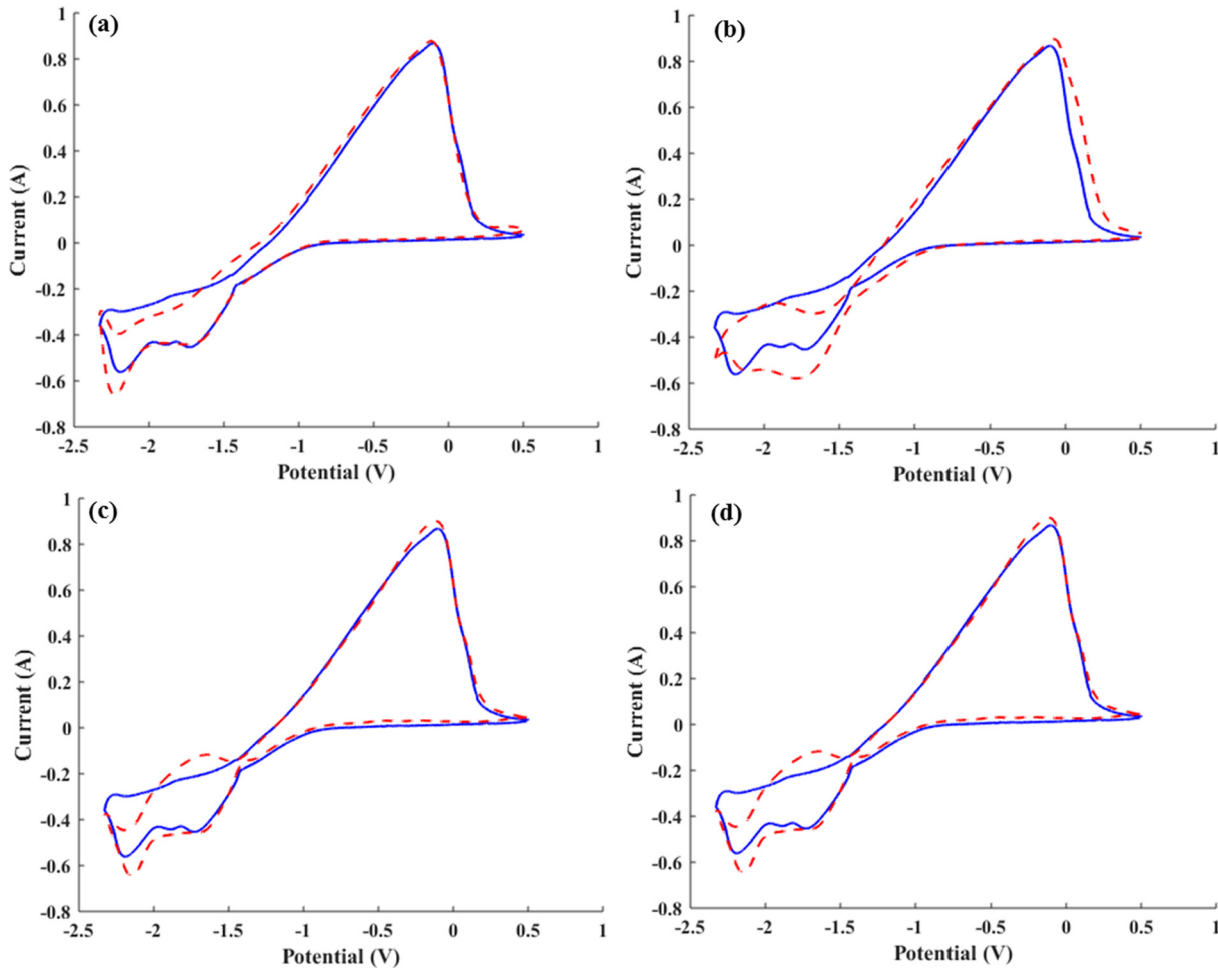


Fig. 15. Comparison of CV plot for 2.5 wt% ZrCl_4 at 400 mV/s, (a): [9, 15, 10]-18 (b): [9, 21, 7]-27, (c): [10, 11, 25]-19, (d): [10, 26, 7]-20 (Blue line = experimental data, Red dash line = ANN prediction). (For interpretation of the references to colour in this figure legend, the reader is referred to the web version of this article.)

different concentrations and scan rates were also explored to illustrate ANN's predictability and limitation. For this purpose, simulated CV curves for 1 wt% ZrCl_4 at 300 mV/s, 2.5 wt% ZrCl_4 at 400 mV/s, and 5 wt% ZrCl_4 at 250 mV/s are superimposed on the actual experimental data, as shown in Figs. 14–16, respectively. Fig. 14 shows that the ANN simulation can capture the important features of the CV graph such as oxidation and reduction peaks very well; few deviations can be seen during the transition from the cathodic sweep to anodic sweep region.

A result from the diffusion model (green line) based from Rakhshan Pouri and Phongikaroon (2016)—using a reverse-engineering program design and coupling various variables to trace the trend of uranium chloride through electrorefinery in a short time—is superimposed in Fig. 14(a) showing its ability to fit the anodic peak. It can be seen that the diffusion model indicates a narrow plot coverage. In addition, when the potential is scanned in negative direction, the CV goes far from the experimental data at approximately -1.0 V . By comparing the result from this study to that from the diffusion model, it is shown that this study provides a good prediction and can display the whole trend of CV with a low error. As seen in Figs. 15(a) and 16(a), the CV plots using [9, 15, 10]-18 structure can capture the beginning of the reduction trend and the oxidation shape well and are comparable to the experimental data sets at high concentrations ($>1\text{ wt\% ZrCl}_4$) as well. Other two structures ([10, 11, 25]-19 and [10, 26, 7]-20) provide a reasonable job in fitting the experimental data sets. However, on the CV plots

with [9, 21, 7]-27 structure (see Figs. 15(b) and 16(b)) fail to capture the reduction features in the higher concentrations.

This outcome leads us to focus on repeatability and distribution of predicted values. Here, based on the results shown in Fig. 11, the best repeatable structure belongs to [9, 15, 10]-18. Thus, to prove this observation, RMSE of predicted values for Figs. 13–16 are compared and listed in Table 3. Table 3 indicates the structure that provides the minimum average RMSE for all tested conditions is related to [9, 15, 10]-18 structure. The next best structure belongs to [10, 11, 25]-19 which shows the average RMSE of 0.0209.

4. Conclusion

We presented a study of data analysis with artificial neural network for the electrorefiner used in pyroprocessing technology. We analyzed zirconium chloride concentrations of 0.5, 1, 2.5, and 5 wt % at different scan rates at 773 K based on the experimental data set of Hoover (2014) and Hoover et al. (2014) to illustrate the ANN ability of handling a complex system. The minimum input data that can be considered as training data is 43% of over 230,000 experimental data points. One, two, and three hidden layers with 1–30 neurons at each layer, and 1–30 validation checks have been analyzed and the minimum average percent error for train and test samples have been calculated. This study proposed

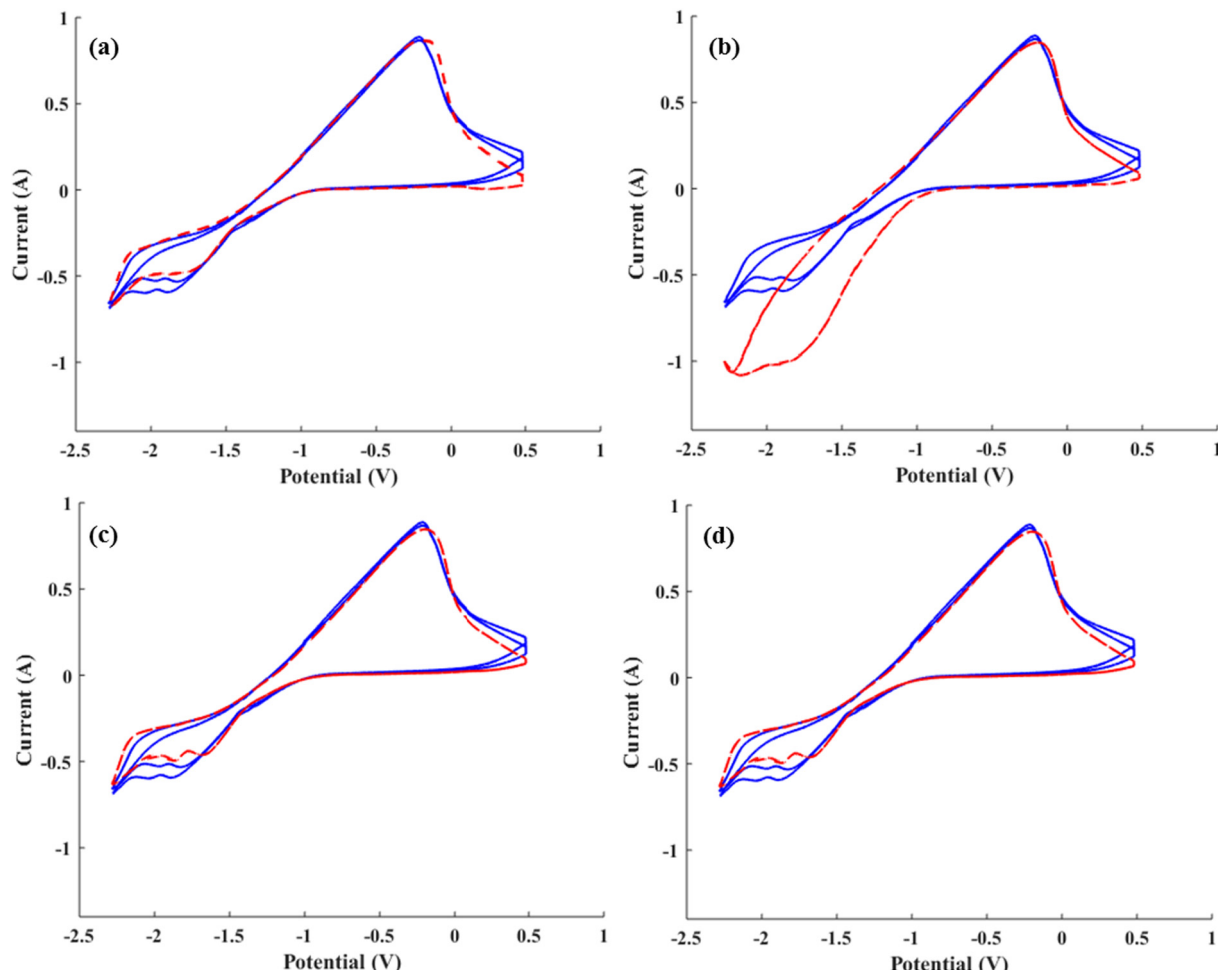


Fig. 16. Comparison of CV plot for 5 wt% ZrCl₄ at 250 mV/s, (a): [9, 15, 10]-18 (b): [9, 21, 7]-27, (c): [10, 11, 25]-19, (d): [10, 26, 7]-20 (Blue line = experimental data, Red dash = ANN prediction). (For interpretation of the references to colour in this figure legend, the reader is referred to the web version of this article.)

Table 3
RMSE for Figs. 13–16.

| Weight percent (wt%), scan rates (mV/s) | (a) [9, 15, 10]-18 | (b) [9, 21, 7]-27 | (c) [10, 11, 25]-19 | (d) [10, 26, 7]-20 |
|---|--------------------|-------------------|---------------------|--------------------|
| 0.5, 450 | 0.00292 | 0.00332 | 0.00366 | 0.00698 |
| 1, 300 | 0.01290 | 0.01713 | 0.01491 | 0.01598 |
| 2.5, 400 | 0.03318 | 0.06175 | 0.03917 | 0.05144 |
| 5, 250 | 0.04392 | 0.21221 | 0.04515 | 0.05822 |

a framework for applying ANN to elide the guessing approach and omit trial and error method. Therefore, the system is able to stop at a reasonable point without going beyond underfitting and overfitting. The results demonstrate that adding hidden layers for a fix training data set results in a smaller learning (modelling) error. The criteria for defining first hidden layer entailed test and train sample which provide the average percent error less than 60% with difference around 5%. For two hidden layers, this scale was tuned to 25% with difference below 2% and for three hidden layers; it is limited to 12% and 1.2%. The average RMSE values of 12 runs for test sample illustrated in Fig. 11 with four mentioned structures can be fallen in 0.004–0.081. This amount for train samples (0.5 wt% at 200 mV/s) is from 0.002 to 0.0032. Two selected structures shown more productive predictions are related to [9, 15, 10]-18 and [10, 11, 25]-19. The results have shown that ANN can be successfully deployed as an alternative method of robust signal detection towards safeguards application in pyroprocessing technology.

Acknowledgment

This work was supported by Nuclear Regulatory Commission Faculty Development through Virginia Commonwealth University.

Appendix A. Supplementary data

Supplementary data associated with this article can be found, in the online version, at <http://dx.doi.org/10.1016/j.anucene.2017.09.002>.

References

- Araromi, Dauda Olurotimi, Afolabi, Tinuade Jolaade, 2007. Neural network control of CSTR for reversible reaction using reverence model approach. Leonardo J. Sci. 6 (10), 25–40.
- Baskin, Igor I., Palyulin, Vladimir A., Zefirov, Nikolai S., 2006. Neural Networks in Building QSAR Models. In: Livingstone, David J. (Ed.), Artificial Neural Networks, Methods in Molecular Biology™, 458. Humana Press, pp. 133–154.

- Bio Logic Science Instrument, 2016. Available: <http://www.bio-logic.net/en/divisions/ec-lab>.
- Burden, Frank, Winkler, Dave, 2009. Bayesian regularization of neural networks. *Method Mol. Biol.* 458, 23–42.
- Evans, Dennis H., O'Connell, Kathleen M., Petersen, Ralph A., Kelly, Michael J., 1983. Cyclic Voltammetry. *J. Chem. Educ.* 60 (4), 290–293.
- Gardner, Matt W., Dorling, Stephen, 1998. Artificial neural networks (the multilayer perceptron) – a review of applications in the atmospheric sciences. *J. Atmos. Environ.* 32 (14–15), 2627–2636.
- Gavin, Henri P., 2016. The Levenberg-Marquardt Method for Nonlinear Least Squares Curve-Fitting Problems, Duke University. Available at <<http://people.duke.edu/~hpgavin/ce281/lm.pdf>>.
- Heinze, Jurgen, 1984. Cyclic voltammetry-electrochemical spectroscopy. *Angew. Chem. Int. Ed.* 23 (11), 831–918.
- Hoover, Robert O., 2014. Uranium and zirconium electrochemical studies in LiCl-KCl eutectic for fundamental applications in used nuclear fuel reprocessing (Ph. D. dissertation). Chemical Engineering department, University of Idaho.
- Hoover, Robert O., Shaltry, Michael R., Martin, Sean, Sridharan, Kumar, Phongikaroon, Supathorn, 2014. Electrochemical studies and analysis of 1–10 wt% UCl₃ concentrations in molten LiCl-KCl eutectic. *J. Nucl. Mater.* 452 (1–3), 389–396.
- Kissinger, Peter T., Heineman, William R., 1983. Cyclic voltammetry. *J. Chem. Educ.* 60 (9), 702–706.
- Koch, Leonard J., 2008. Experimental Breeder Reactor-II (EBR-II): An Integrated Experimental Fast Reactor Nuclear Power Station. American Nuclear Society, La Grange Park, Illinois.
- Kriesel, David, 2007. A Brief Introduction to Neural Networks. Available from: <http://www.dkriesel.com/_media/science/neuronalenetze-en-zeta2-col-dkrieselcom.pdf>.
- Lahiri, Sandip, Ghanta, Kartik Chandra, 2010. Artificial neural network model with parameter tuning assisted by agentic algorithm technique: study of critical velocity of slurry flow in pipeline. *Asia-Pac. J. Chem. Eng.* 15 (2), 763–777.
- Laidler, James J., Battles, J.E., Miller, W.E., Ackerman, J.P., Carls, E.L., 1997. Development of pyroprocessing technology. *Process. Nucl. Energy* 31 (1–2), 131–140.
- Lawrence, Steve, Lee Giles, C., Ah Chung, Tsoi, 1997. Lessons in neural network training: overfitting may be harder than expectedProceedings of the Fourteenth National Conference on Artificial Intelligence, AAAI-97. AAAI Press, Menlo Park, California, pp. 540–545 (1997).
- Mabbott, Gary A., 1983. An introduction to cyclic voltammetry. *J. Chem. Educ.* 60 (9), 697–702.
- Manic, Milos, Sabharwall, Piyush, 2011. Computational Intelligence as a Tool for Small Modular Reactors. Small Modular Reactors Symposium (SMR), Washington DC, September, pp. 28–30.
- Nicholson, Richard S., 1965. Theory and application of cyclic voltammetry for measurement of electrode reaction kinetics. *J. Anal. Chem.* 37 (11), 1351–1355.
- Oark, Jaeyeong, Choi, Sungyeol, Sohn, Sungjune, Kim, Kwang-Rang, Hwang, Soon, 2014. Cyclic voltammetry on zirconium redox reactions in LiCl-KCl-ZrCl₄ at 500° C for electrorefining contaminated zircaloy-4 cladding. *J. Electrochem. Soc.* 161 (3), H97–H1054.
- Planche, Alejandro Speck, Cordeiro, Natalia D.S., 2015. A general ANN-based multitasking model for the discovery of potent and safer antibacterial agents. *Methods Mol. Biol.* 1260, 45–64.
- Rakhshan Pouri, Samaneh, Phongikaroon, Supathorn, 2016. Investigation on Reactions Probabilities for Cyclic Voltammetry of Zirconium in LiCl-KCl Eutectic Molten Salt via Reverse-Engineering Method. American Nuclear Society (ANS), Annual Meeting, New Orleans, LA, June 12–16.
- Ridluan, Ardit, Manic, Milos, Tokuhiro, Akira, 2009. EBaLM-THP-a neural network thermo hydraulic prediction model of advanced nuclear system components. *Nucl. Eng. Des.* 239 (2), 308–319.
- Samin, Adib, Lahti, Erik, Zhang, Jinsuo, 2015. Analytical solution of the planner cyclic voltammetry process for two soluble species with equal diffusivities and fast electron transfer using the method of eigen function expansion. *AIP Adv.* 5 (8), 087141.
- Samin, Adib, Wang, Zhonghang, Lahti, Erik, Simpson, Michael, Zhang, Jinsuo, 2016. Estimation of key physical properties for LaCl₃ in molten eutectic LiCl-KCl by fitting cyclic voltammetry data to a BET-based electrode reaction kinetics model. *J. Nucl. Mater.* 475, 149–155.
- Simpson, Michael F., Law, J.D., 2010. Nuclear Fuel Reprocessing, Fuel Cycle Science and Technology Division, Idaho National Laboratory, INL/EXT-10-17753.
- Siriphala, Phermsak, 2000. Controlling artificial neural networks overtraining when data is scarce (Ph.D. dissertation). Wichita State University, Department of Industrial and Manufacturing Engineering.
- Taylor, Brian, Darrah, Marjorie, Moats, Christina, 2003. Verification and Validation of Neural Networks: a Sampling of Research in Progress. International Society for Optical Engineering (SPIE), Intelligent Computing: Theory and Applications, 5103 (8), August 7.
- Wijayasekara, Dumudu, Manic, Milos, Sabharwall, Piyush, Utgikar, Vivek, 2011. Optimal Artificial neural network architecture selection for performance prediction of compact heat exchanger with the EBaLM-OTR technique. *Nucl. Eng. Des.* 241 (7), 2549–2557.
- Williams, Ammon N., 2016. Measurment of Rare Earth and Uranium Elements Using Laser-induced Breakdown Spectroscopy (LIBS) in an Aerosol System for Nuclear Safeguards Applications (Ph.D. dissertation). Mechanical and Nuclear Engineering Department, Virginia Commonwealth University.